

11-2-2015

Kelvin Probe Electrode for Field Detection of Corrosion of Steel in Concrete

Leonidas Philip Emmenegger

University of South Florida, lemменegger@mail.usf.edu

Follow this and additional works at: <http://scholarcommons.usf.edu/etd>

 Part of the [Civil Engineering Commons](#)

Scholar Commons Citation

Emmenegger, Leonidas Philip, "Kelvin Probe Electrode for Field Detection of Corrosion of Steel in Concrete" (2015). *Graduate Theses and Dissertations*.

<http://scholarcommons.usf.edu/etd/5944>

This Thesis is brought to you for free and open access by the Graduate School at Scholar Commons. It has been accepted for inclusion in Graduate Theses and Dissertations by an authorized administrator of Scholar Commons. For more information, please contact scholarcommons@usf.edu.

Kelvin Probe Electrode for Field Detection of Corrosion of Steel in
Concrete

by

Leonidas P. Emmenegger

A thesis submitted in partial fulfillment
of the requirements for the degree of
Master of Science in Civil Engineering
Department of Civil and Environmental Engineering
College of Engineering
University of South Florida

Major Professor: Alberto A. Sagiúes, Ph.D.
Stanley C. Kranc, Ph.D.
Stephen E. Sadow, Ph.D.

Date of Approval:
October 27, 2015

Keywords: Novel Method, Potential Mapping, Continuous Measurement, Mobile, NCHRP

Copyright © 2015, Leonidas P. Emmenegger

ACKNOWLEDGMENTS

The author acknowledges the contributions made by Distinguished University Professor Dr. Alberto A. Sagüés, who took upon himself the additional work and commitment in serving as the Major Professor, and who was available and willing to provide assistance, direction, and general support of the project.

The author gratefully acknowledges the scholarship support from funds from the National Academies, National Academy of Science National Cooperative Highway Research Program, Contract No. NCRHP-176 of the Highway IDEA Program.

The author would like to thank his fellow Graduate Research Assistants (Especially: Andrea Ramirez, Enrique Paz, Michael T. Walsh, Jacob Bumgardner) along with undergraduates who participated in the project as part of USF's Research Experience for Undergraduates (William Ruth, Connor Fries, Ihab Taha, Tafadzwa Chigumira).

Lastly, the author would like to acknowledge the support and encouragement provided by his family.

TABLE OF CONTENTS

LIST OF TABLES	ii
LIST OF FIGURES	iii
ABSTRACT	v
CHAPTER 1: INTRODUCTION	1
CHAPTER 2: PRINCIPLE OF OPERATION AND PROBE DESIGN	10
2.1 Principle of Operation	10
2.2 Probe Components	12
2.2.1 Capacitance of a Mesh Disk Compared to that of a Solid Disk	14
2.2.2 Measurement of the Capacitances of the Disk-Plate Systems	14
2.2.3 Calculating Theoretical Values of Capacitance for the Disk-Plate Systems	16
2.3 Probe Control System	20
2.4 Probe Design	23
2.5 Dynamic Probe Response and Proposed Method for Further Signal Processing	27
2.5.1 Proposed Method for Improved Signal Processing	28
CHAPTER 3: LABORATORY SCALE INDOOR TESTING	33
3.1 Laboratory Testing on Concrete Slabs	33
3.1.1 Laboratory Testing Experimental Objective and Methodology	34
3.1.2 Laboratory Testing Experimental Results	35
CHAPTER 4: OUTDOOR LARGE SCALE TESTING	38
4.1 Potential Map Generation	38
4.1.1 Potential Map Generation Results	40
CHAPTER 5: SUMMARY OF FINDINGS	45
REFERENCES	47

LIST OF TABLES

Table 1-KP Components with Descriptions	13
Table 2-Comparison of Capacitance to Plate of Mesh and Solid Disks	18

LIST OF FIGURES

Figure 1 Polarization diagram.....	3
Figure 2 Reference electrode potential mapping	4
Figure 3 Schematic of a Kelvin Probe (KP)	6
Figure 4 Laboratory-scale probe used by [1].....	8
Figure 5 Future KP array of multiple probes used to scan an entire bridge lane in one pass	9
Figure 6 Schematic of the KP System	10
Figure 7 Solid disk test configuration.....	15
Figure 8 Mesh disk test configuration close-up image	16
Figure 9 Comparison of idealized configuration and actual results	19
Figure 10 DPS schematic outlining the major components and their relation to each other.....	21
Figure 11 Block diagram of the LabVIEW™ code	22
Figure 12 Nulling zero process	22
Figure 13 Schematic of the KP Prototype emphasizing major components.....	24
Figure 14 KP on concrete slab with emphasis on Data Processing Unit	25
Figure 15 The vibrator and other key frame components.....	25
Figure 16 Photo of the underside of the KP.....	26
Figure 17 Distance transducer	26
Figure 18 Probe-time response for a potential step	28
Figure 19 Measured potential profile versus actual potential profile	29
Figure 20 Probe-time response schematic	29

Figure 21 Schematic of the laboratory experimental setup	33
Figure 22 Laboratory concrete beam test setup	34
Figure 23 Potential profiling.....	35
Figure 24 Short term reproducibility tests	37
Figure 25 Instrumented test slab schematic	38
Figure 26 Photo of the testing apparatus with the MKPP.....	39
Figure 27 Setup employed when scanning the reinforced concrete slab	40
Figure 28 For a given row of the slab the above potential profiles were measured using the MKPP	41
Figure 29 Potential maps generated using the MKPP and traditional method	42
Figure 30 Sample calibration from previous scanning of the concrete slab under similar conditions	44

ABSTRACT

While the Kelvin Probe (KP) has been used in a variety of surface scanning applications, the use of the KP in reinforced concrete structures to detect corrosion has been pioneered by previous work performed at the University of South Florida. However, in that work, the scale and construction of the probes was not suited to use in the field. This is primarily attributable to the small operating disk-to-concrete gap which would make the probe unable to accommodate road conditions, such as irregularities in the grading of the road, and local pitting of the surface. Therefore, it was important to investigate whether the KP can be scaled up while still maintaining resolution and fidelity of the measurements taken. The new mobile KP prototype (MKPP) constructed in this work, has a sensing disk that is approximately 10 cm in diameter and is capable of operating up to 2 cm above the concrete surface. Testing consisted of mapping an instrumented test slab simulating a corroding concrete bridge deck, at a rate of travel of about 0.6 mph (~1 ft/s) over the slab surface. The potential map generated through use of the MKPP successfully identified the corroding spot, the location of which was verified using the traditional half-cell potential mapping method outlined in ASTM C 876-09. The MKPP mapping in these trials was approximately 10 times faster than when using the traditional method. The faster potential mapping by the MKPP, while still identifying corroding sites, should allow for more economical and less intrusive survey of the condition of bridge decks. The work set the necessary proof of concept for future demonstration of an array of such probes which would further magnify the beneficial effect.

CHAPTER 1: INTRODUCTION

Concrete and steel are used widely in construction globally. Concrete is often reinforced with steel to prevent cracking, improve its durability, and to impart tensile strength [2]. The steel normally does not corrode significantly because of the presence of a protective thin surface passive film, which forms due to the high pH of the concrete pore water [3]. However, chloride ions can cause film breakdown resulting in steel corrosion [3]. As the steel in the concrete corrodes, a large net volume expansion (e.g. 400%) can occur at the corrosion sites which results in local tensile stresses in the concrete. The concrete's tensile strength, which is approximately 10% of its compressive strength, is only ~400 psi [4], which is insufficient to resist the corrosion-induced tensile stresses. Hence, corrosion of the steel reinforcement causes the concrete to crack and delaminate [5] resulting in the need for expensive maintenance repairs.

Corrosion causes a heavy financial toll. According to a U.S. Federal Highway Administration (FHWA) 2002 study done in conjunction with NACE International (the corrosion society), corrosion in the U.S. has a direct cost of approximately \$276 billion annually [6]. Of special interest is the case of corrosion in bridges, a key component of the civil infrastructure. There are approximately 600,000 bridges in the United States and according to a 2006 Federal Highway Administration Report, roughly 70,000 or 11.7% of bridges are in what the report describes as a "structurally deficient" condition [7][5].

A key point in controlling corrosion of steel in concrete is determination of the corrosion sites. Corrosion is not uniform in most cases, but rather is dispersed over a number of active sites. Steel undergoing corrosion (at an active site) develops a relatively high negative potential

with respect to the surrounding concrete (when measured with a reference electrode, usually a Cu/CuSO₄ electrode [8]), in the order of hundreds of millivolts. The causes for the differences in electrical potential between corroding and passive sites will be expanded on below.

When the steel corrodes the two primary reactions involved are iron oxidation (Eq. (1)) and oxygen reduction (Eq. (2)), representing the anodic and cathodic reactions respectively.



The anodic reaction liberates electrons, and in the absence of additional sinks or sources of electrons, the electrons are then consumed by the cathodic reaction. Therefore under steady state conditions, without external influence, the reaction rate of the cathodic and anodic reactions are equal. When describing corrosion, it is customary to talk in terms of current densities rather than reaction rates. The current density is a measure of the electrical current divided by the area over which it is applied (in units of A/cm² for example). For a particular reaction, the current density “i” can be described using the Faradaic conversion which relates the current generated over time to the moles of electrons that have been transferred:

$$i = nF * (Reaction Rate) \quad (3)$$

where “n” is the number of valence electrons for the species (2 in the case of iron), “F” is Faraday’s constant (96500 coulombs/ mol of electrons). Using current densities, the relationship between the anodic and cathodic reaction under steady state can be represented by convention as -i_a = i_c, where i_a and i_c are the anodic current density and cathodic current density respectively. It is important to note that as the potential of the steel varies, the rates of the anodic and cathodic reactions tend to change exponentially as described by Tafel [9][10]. More specifically, as the

potential of the steel becomes more negative by, for example, a few hundred millivolts, i_a increases by orders of magnitude, whereas i_c decreases by orders of magnitude (this can be visualized as the anodic reaction curve in Figure 1 shifting left or right) [9]. By plotting the anodic and cathodic current densities as a function of the potential of the steel, a polarization diagram is as seen in Figure 1 below. The intersection of the two curves represents the stable; steady state condition described earlier, wherein the cathodic reaction consumes the electrons liberated by the anodic reaction.

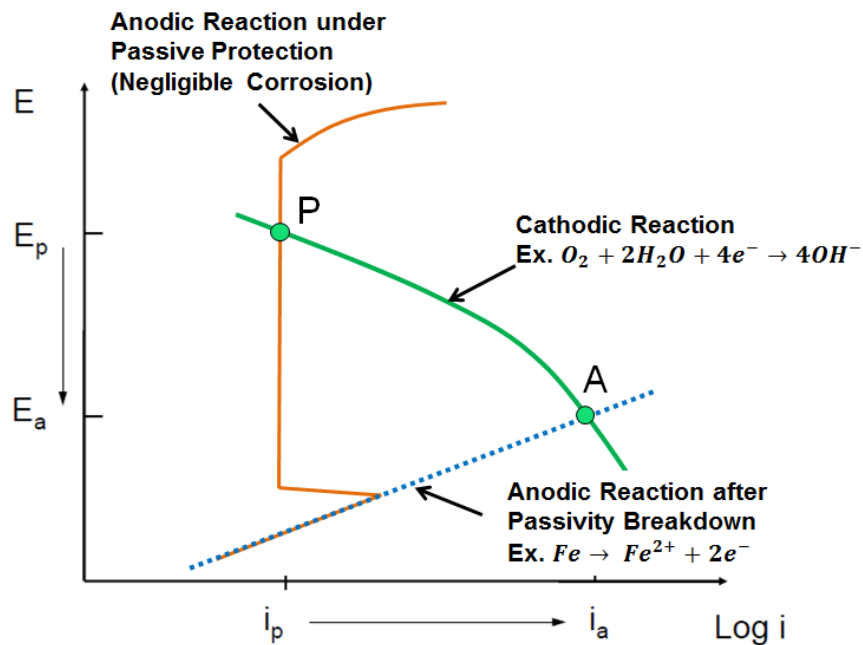


Figure 1-Polarization diagram. A polarization diagram plots the potential of the steel versus the surrounding medium under various cathodic and anodic reaction conditions. Note that as convention dictates, the current densities (i_a and i_p) are plotted on log scale.

When the steel is passive, the anodic current density is exceedingly small, and the point of intersection between the two current densities (i_a and i_c) occurs at a nobler potential (E_p) as denoted by the intersection point P on the polarization diagram shown in Figure 1. When the

passive layer breaks down and corrosion is prevalent, the anodic reaction rate is higher and the cathodic reaction intersects much lower leading to a more negative potential.

In an extended corroding system, by locating the points of relatively negative potential (such as -400 mV compared to -100 mV for example), determination of the corroding sites is possible. The potential is usually measured against a reference electrode that is systematically placed along the concrete at various points [8]. The resulting data set plotted as a 2D surface map showing the various potentials of the concrete surface, is referred to as a potential map. It is primarily by this method that determining the location of corroding sites of the steel reinforcement in the concrete not plainly visible is customarily done.

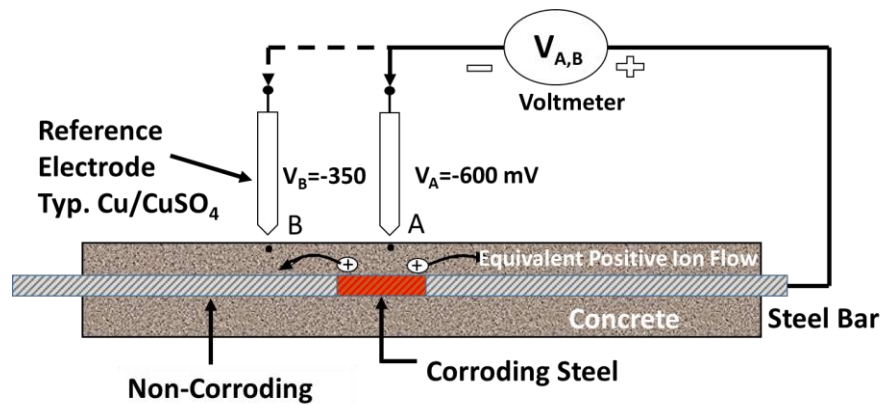


Figure 2- Reference electrode potential mapping. The reference electrode is placed at point A (corroding site) then moved to point B (passive site) and a nobler potential is measured at point B.

Corrosion results in an equivalent positive ionic current flow from the corroding steel zone to the nearby non-corroding steel zones [11]. Consider the case where the reference electrode is initially in contact with the concrete surface at point A (beneath which actively corroding steel exists) then subsequently placed at point B, over non-corroding steel. Reflecting the ionic flow, the concrete surface at position A is more positive than at position B, so the

voltmeter will register the difference, and identify position A as a corroding site. Note that due to the customary voltmeter connection polarity, shown in Figure 2 (positive terminal attached to the steel bar and the negative terminal attached to the reference electrode), the voltmeter readings exhibit the opposite relationship from that of the surface potentials so the reading obtained for position A is more negative than for position B. Thus, despite the fact that position A is a positive ion source, due to the way in which the voltmeter is connected, A will have a measured potential that is more negative with respect to the steel than the potential measured at position B. The reference electrode contains at one end a metallic terminal that is connected to the voltmeter, while the other end has a wet-tip which must contact the surface of the concrete (commonly through a moist sponge), where the tip interacts with the electrolyte in the concrete pores at that point. As noted in [1] detrimental issues with wet-tip electrode potential measurement are: the disturbance caused by the ions from the electrolytic solution of the reference electrode mixing with and altering the amount of the electrolyte solution in the pores, scatter in measurements depending on the initial water saturation level of the pores in the concrete surface, and consequently, the sometimes relatively long time for the system to stabilize before obtaining a measurement. Work by [1] demonstrated that a wet-tip electrode concrete surface potential measurement can drift as much as 40 mV over the span of three minutes.

It is in part to address the shortcomings noted above that a novel method for measuring potential differences on a concrete surface was developed [1]. The new method centers on the use of a Kelvin Probe (KP) electrode, which as will be shown next, has no direct contact with the concrete surface, and therefore doesn't interfere with the concrete surface as in the case of a conventional electrode. In addition the KP produces measurements that are nearly instantaneous, stable, and reproducible.

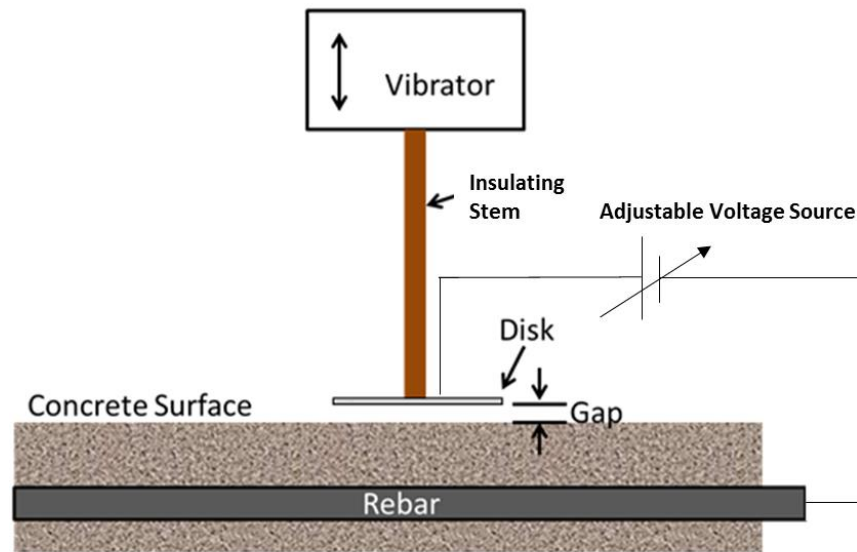


Figure 3-Schematic of a Kelvin Probe (KP).

The KP is a tool used for the measurement of potential difference (PD) between two conductors [12]. If the conductors are metallic and simply in contact with each other without any impressed current, the PD is equal to the difference of the work functions of the two conductors [12]. For the case of steel in concrete one of the conductors is in the form of a metal disk that is in electrical contact (through other intermediate components) with the reinforcing steel, while the other conductor is the surface of the concrete. By measuring the difference of potential of the disk with respect to the concrete at two different points on the concrete surface, one can infer the difference of potential between those two different points and hence identify corroding spots. A more rigorous explanation of the electrochemical interactions involved with a KP system can be found in [1]. The metal disk is placed close to, but not touching, the surface of the concrete effectively forming a parallel plate electrical capacitor. The natural potential difference “ V_n ” between the disk and the concrete surface results in an associated electric charge “ Q ” of the

capacitor, following the usual relationship: $Q = C * V_n$, where “C” is the value of the capacitance [13]. The value of C depends primarily on the distance “h” between the plates. If that distance is made to vary, for example by attaching the metal disk to a vibrating stem, the value of Q will vary in concert with the vibration frequency. The charge variations are transmitted through the contact chain between the disk and the reinforcing steel, in the form of an alternating current (AC). If the electrical contact between the disk and the reinforcing steel is broken and an adjustable voltage source (of value “Va”) is inserted in the circuit, the potential difference in the capacitor is altered accordingly, and the alternating current intensity can be increased or decreased as a result. If the voltage source is adjusted so that Va exactly equals -Vn, the alternating current vanishes. This arrangement then offers a means of measuring Vn by recording the value of Va when a null value of current is achieved. The principle of operation described above will be elaborated on in Section 2.1. The process can be performed automatically with ordinary electronic circuitry. Thus, a measurement of concrete surface potential differences can be made without touching the surface, by placing the vibrating disk over various points on the concrete surface [1].

Recent work by Sagüés and Walsh [1] demonstrated the applicability of the KP to the measurement of potentials on a concrete surface. Figure 4 shows the underside of the probe constructed for that investigation. The disk vibration was achieved by attaching the stem to the vibrating diaphragm of a small loudspeaker (voice coil). An electronic front end circuit, also known as a preamplifier, (modeled on that published by Klein [12]) was used to condition the disk signal.

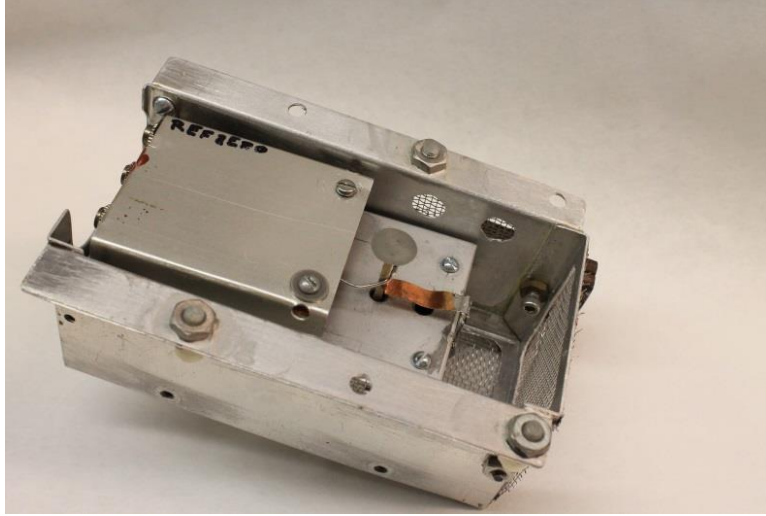


Figure 4-Laboratory-scale probe used by [1].

The experiments detailed in [1] demonstrated that the probe was able to measure potentials on concrete in a replicable fashion with very low potential drift, and that the potential measured by the probe was that of the concrete surface and not at a plane deeper into the concrete. The tests also showed that the potential measurements were only moderately dependent on the disk-to-concrete gap. The probe embodiment used for those experiments was however a small laboratory unit, with a very small diameter disk (~13 mm) and a very short disk-to-concrete surface distance (~1mm); useable only on very smooth laboratory concrete surfaces. Vibration frequency was ~160 Hz and vibration amplitude was ~0.5 mm. Extension of the probe concept to applications in the field with rough concrete surfaces and other realistic conditions is the subject of proprietary work covered by provisional patent applications filed by USF [14]. Among those concepts are the recognized needs for increasing the size of the sensing element and disk-to-concrete gap to the concrete surface by about one order of magnitude, implementation of a metal mesh disk to minimize mass and air movement, and exploring the feasibility of controlling that distance by automatic means [14].

Additionally, as part of the work scope of NCHRP IDEA Project 176, the project which this thesis is based on, future work will demonstrate feasibility of coordinated operation of more than one probe, toward future concepts for mounting multiple KP's in an array for faster survey of bridge decks. This concept is patent pending [14], and is presented here for the purpose of describing possible future uses of the KP technology described in this thesis. Figure 5 shows the diagram presented in the patent application showing what an array of Kelvin Probes might look like for the purposes of scanning bridge decks.

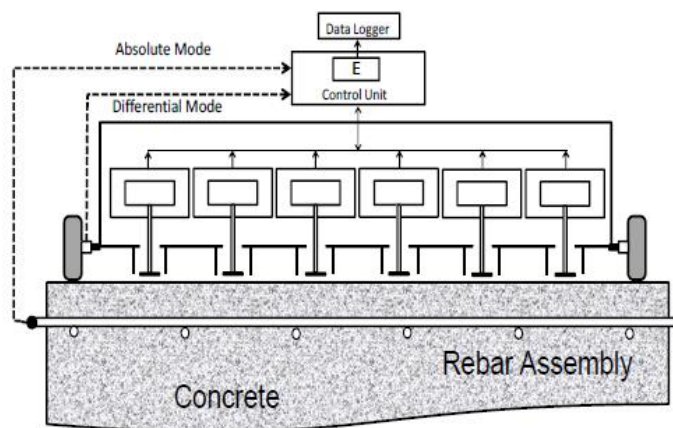


Figure 5-Future KP array of multiple probes used to scan an entire bridge lane in one pass. Multiple probes were used so as to allow for a larger area to be scanned without losing resolution and for practical purposes [14]. Patent Pending.

The objective of the investigation addressed in this thesis is to design, develop and assess a scaled-up, mobile Kelvin Probe prototype for practical potential profiling on large concrete surfaces, to serve as basis for future field applications. In implementing the recognized needs described in the introduction above and toward achieving the project objectives, principles of operation and probe design related to addressing scaling up of the laboratory unit [1] to the field model are presented in the next chapter. Implementation and field probe prototype operation are presented in subsequent chapters.

CHAPTER 2: PRINCIPLE OF OPERATION AND PROBE DESIGN

2.1 Principle of Operation

The KP sensing disk facing the concrete surface was modeled for simplicity as an ideal parallel plate capacitor. An ideal parallel plate capacitor consists of two plates placed at some small distance (relative to the size of the plates) from each other. It is assumed that the electric field in the gap is uniform, which is equivalent to treating the conductors as charged infinite sheets. In reality the KP sensing disk is finite in size, however for the smaller gap sizes relative to its diameter the results from such an approximation should not deviate much from actual conditions; at larger gaps the behavior is more complicated as shown in the next section. Figure 6 is a simplified schematic of the system.

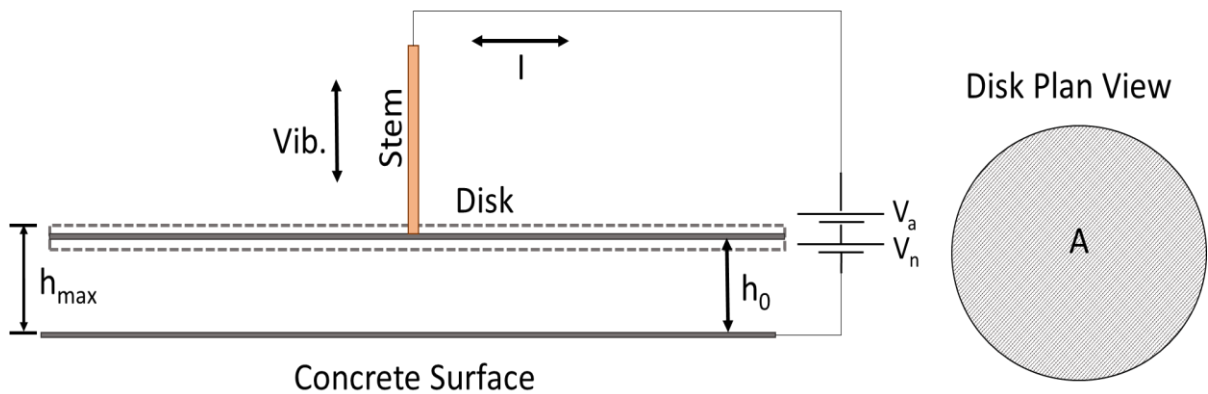


Figure 6- Schematic of the KP System.

As mentioned in the Introduction, for an ideal parallel plate capacitor the charge Q , is given by the following equation [13]:

$$Q = C * V \quad (4)$$

where C is the capacitance, and V is the potential difference between the disk and the concrete surface at any given moment, and can be more accurately described by the relationship:

$$V = V_n + V_a \quad (5)$$

where V_n is the natural potential difference between the disk and the concrete surface and V_a is the potential applied in the nulling process. When the current is nulled, $V_a = -V_n$. Additionally, the capacitance C for an ideal parallel plate capacitor is given by the following equation [13]:

$$C = \frac{\epsilon\epsilon_0 A}{h} \quad (6)$$

where C is the capacitance, measured in Farads, ϵ is the dielectric constant of the intervening medium (assumed to be air, with $\epsilon \sim 1$) between the capacitor's conductors, ϵ_0 is the free space permittivity (8.854×10^{-12} F/m), A is the one-sided cross-sectional area of the disk, and h is the distance between the conductors. Substitution of Eq. (6) into Eq. (4) yields the following expression for the charge in the system at a given moment:

$$Q = \frac{\epsilon\epsilon_0 AV}{h} \quad (7)$$

An AC current is generated when cyclically varying, by a small amount, the perpendicular distance between the two conductors, by means of a mechanically vibrating driver. Taking the time derivative of the above expression will yield the expression of current in the system as:

$$I(t) = \frac{-\epsilon\epsilon_0 AV}{h^2} \frac{dh}{dt} \quad (8)$$

Note that dh/dt is the difference between h_{\max} and h_{\min} . Defining a constant K that will have the form:

$$K = -\varepsilon\varepsilon_0 \quad (9)$$

The final governing equation for the current is:

$$I(t) = \frac{KAV}{h^2} \frac{dh}{dt} \quad (10)$$

The following observations are readily made upon examination of Eq. (10), assuming for simplicity a sinusoidal vibration condition and treating $I(t)$ as a simple alternating current:

- 1) The current amplitude decreases by the square of the distance between the plates.
- 2) The current's amplitude increases proportionally with an increase in A , V , and dh/dt .

Using those observations, it becomes apparent that a significant increase in the gap size between the disk and the concrete surface (a project goal described in the Introduction) (h) must be offset by a large increase in either the cross-sectional area of the disk (A), or an increase in the vibration amplitude for the same or relatively similar current to be achieved. It is highly desirable to increase the gap size as a means of accommodating for irregularities in the road surface such as an uneven surface, which is likely present in field conditions. Consequently, the cross-sectional area of the disk needed to be made larger as the gap size was increased from 1 mm that [1] employed in their prototype, to the 1 cm established for this probe. Consequently, the disk diameter was increased by an order of magnitude with respect to the diameter of the disk used on the laboratory scale probes used by [1].

2.2 Probe Components

The probe is made of the key components listed in Table 1.

Table 1- KP Components with Descriptions

Major Component	Purpose/Description
Sensing Disk	Serves as half of the parallel plate capacitor that facilitates the inducement of the current that will be nulled by the system.
Preamplifier	Amplifies the current signal generated through perpendicular vibration of the sensing disk over the concrete surface and conditions the signal.
Electromechanical Vibrator	Provides the physical movement of the disk.
Data Processing Unit	Consists of a Dell Inspiron computer running the LabVIEW™ code used for operation of the probe.
Distance Transducer	Determines the distance the probe traveled.

A schematic of the probe components found in Table 1 can be found in Section 2.4 as Figure 13. The preamplifier and the electromagnetic vibrator are preassembled components that will not be discussed in detail here. The distance transducer was designed and constructed for the project by Dr. Michael Celestin, a senior research engineer of the College of Engineering of the University of South Florida. The shield is simply a Faraday cage that is used to isolate the sensing disk from some of the environmental noise, a description of the mechanism by which Faraday cages work is present in [15]. The sensing disk and the data processing unit were customized components that are described in the following sections. The response of the probe to transient inputs was of particular concern as it limits the speed of operation and merits special consideration in a next subsection as well.

2.2.1 Capacitance of a Mesh Disk Compared to that of a Solid Disk

Section 2.1 indicated the need for a larger disk to offset the reduction in current that is a consequence of increasing the gap between the sensing disk and concrete from about 1 mm to 1 cm. As a consequence of increasing the diameter of the sensing disk, considerations needed to be made to mitigate secondary detrimental effects that become more pronounced as the disk diameter increases. Those effects may include, fanning consequences, wherein the rapid movement of the larger cross-section causes significant air movements that may enhance non-uniform tilt vibration, or interfere with the potential measurement by altering surface humidity, and an increased mass of the disk which burdens the system and reduces the achievable amplitude of vibration. As described in the patent application cited [14] a wire mesh construction as opposed to a solid bulk sensing disk was proposed. Consequently, a mesh disk configuration was chosen. Because the capacitance of a mesh disk/ solid plane capacitor is expected to be less than that of a solid disk/solid plane capacitor, an investigation was performed to ascertain whether the AC generated per Eq. (10) through perpendicular vibration of the mesh disk over the concrete surface will be sufficiently large to allow for appropriate operation. To quantify the loss in capacitance in using a mesh disk as opposed to a solid disk, both an empirical (Section 2.2.2) and a theoretical assessment (Section 2.2.3) were performed.

2.2.2 Measurement of the Capacitances of the Disk-Plate Systems

To empirically determine the decrease in capacitance in going from a solid disk to a mesh, two approximately circular disks, one mesh and the other solid of nearly the same diameter (about 10 cm) were alternatively held above a somewhat larger flat metallic plate conductor. On first approximation it was assumed that the electric field generated is uniform and

perpendicular to the plate, but this assumption loses validity the further the disk is separated from the plate in the experimental setup. Hence, the measurements were limited to distances less than $\sim 1/5$ of the disk diameter. The capacitance of each disk-plate combination was measured at various distances of separation using a Hewlett Packard 4192ALF Impedance Analyzer in a 2-point configuration, and operating at a frequency of 100 kHz. Figures 7 and 8 illustrate the experimental setup with the solid and mesh disks in place respectively. The 22-gauge connecting wires between disk and plate and the impedance analyzer were about 1.5 ft (45.7 cm) long each. The effect of added capacitance of the wires, estimated to be in the order of $< 4\text{pF}$, was subtracted from the measured values.

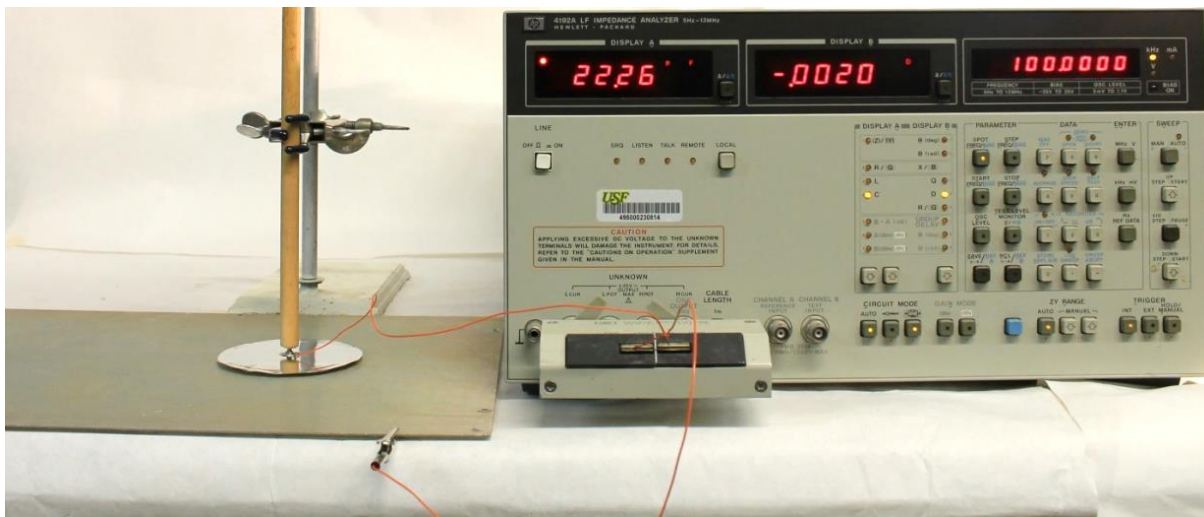


Figure 7-Solid disk test configuration.

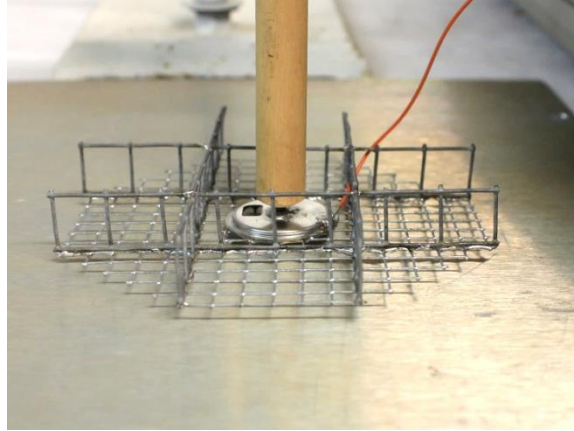


Figure 8-Mesh disk test configuration close-up image. The disk shown was eventually adopted as the new sensing disk for the unit.

The diameters of the solid and mesh disk were 9.8 cm and 10 cm respectively. The solid disk was made out of steel sheet ~0.254 mm thick. The mesh disk was made of two galvanized steel mesh. The primary mesh (for the actual disk surface) has a wire diameter of 0.021 in (0.53mm) in a square 1/4 in (6.4 mm) grid. The metal plate, of aluminum alloy, was 32 cm by 42 cm with a thickness of 0.002 cm. The metal plate was much larger than either of the disks so it approached an infinite plane configuration to aid in producing a more uniform electric field between the conductors.

2.2.3 Calculating Theoretical Values of Capacitance for the Disk-Plate Systems

Estimation of the capacitance between the solid disk and metal plate was done by means of Eq. (6) using the one-sided cross-sectional area of the solid disk, being that it is the smaller of the two components and hence the one most determining the region of the highest and most uniform electric field.

In the case of the mesh disk, Eq. (6) is not applicable due to the complex electric field resulting of the geometry of the mesh. Rather, the following expression was found to be most

applicable, and is based on an equation which was developed for use in calculating the capacitance to ground of an array of parallel cylindrical wire-like elements parallel to the ground [16]:

$$C = \frac{\epsilon_0}{b + \frac{a}{2\pi} \ln \frac{a}{2\pi r}} * A \quad (11)$$

where “C” is the capacitance of the mesh-bottom plate system, “r” is the wire radius (taken here as that of an equivalent round wire), “a” is the center-to-center distance between neighboring parallel wires, “b” is the distance between the wire’s centerline and the ground plane, and A is the overall footprint of the array. In our case r was assumed to be 0.265 mm, ½ of the equivalent diameter mentioned above. Since the mesh employed was not composed of parallel wires, an effective value of “a” needed to be estimated. Eq. (11) assumes an array of parallel wires, therefore the square grid was mathematically converted to an approximately equivalent array of parallel wires of spacing 3.2 mm. Geometric calculations showed that 3.2 mm spacing approximated the placement density using parallel wires contained within the perimeter of the disk (and no wire on the perimeter) .

The following calculations were made for a series of values of the separation h between disk and plate:

- 1) Idealized capacitance (column 3), using Eq. (6) between the solid disk and the plate.
- 2) Idealized capacitance (column 6), using Eq. (11) between the mesh disk and the plate.
- 3) Percent difference between the result of the measured capacitance of the solid disk/plate system and the idealized capacitance (column 4) determined by (a): $100 * (\text{Measured} - \text{Idealized})/\text{Idealized}$.

4) Percent difference between the result of the measured capacitance of the mesh disk/plate system and the idealized capacitance (column 7) determined by (b) $100 * (\text{Measured} - \text{Idealized})/\text{Idealized}$.

5) Percent difference between the result of the measured capacitance of the mesh disk/plate system and that determined for the solid disk/plate system (column 9): $100 * (\text{Mesh-Solid})/\text{Solid}$.

Table 2- Comparison of Capacitance to Plate of Mesh and Solid Disks

Separation Dist. "h" (cm)	Solid Disk (9.8 cm Diameter Disk)			Mesh Disk (10 cm Diameter Disk)			Solid Disk vs. Mesh Disk		
	Observed Cap. (pF)	Idealized Cap. (pF)	% Diff.	Obs. Cap.	Ideal. Cap.	% Diff.	ΔC Obs. Values (pF)	% Diff.	
0.5	16.6	13.4	24.4	16.0	13.1	22.7	0.60	-3.6	
1	8.1	6.7	21.6	7.9	6.7	17.7	0.20	-2.4	
2	4.7	3.3	39.4	4.0	3.4	17.4	0.64	-13.7	
							Avg:	0.48	-6.6

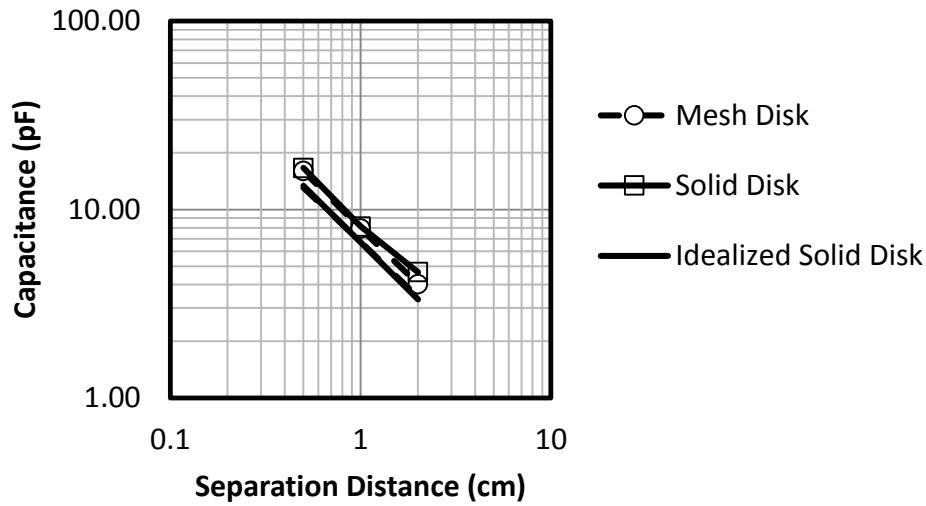


Figure 9-Comparison of idealized configuration and actual results.

Selected results in Table 2 are shown graphically in Figure 9. Several observations apply. First, there was good agreement (less than an order of magnitude difference) between the idealized and measured capacitance values. The result validates the assumption that at small separation the field between disk and plate approached well that which corresponded to an infinitely wide system, and confirmed that the measurements were performed correctly. Second, over the range of separation distances investigated there was an approximately constant relative deviation between the capacitance for the solid disk and that for the mesh, the latter being on average about 93 % of the former.

As can be seen in Eq. (10) the current received at the preamplifier of the system is linearly proportional to the capacitance. The small reduction in capacitance caused by using a mesh disk (~7 %) should not prevent full system operation.

If the gap between the surface and the disk is increased further, the instrumental approach has to be reevaluated to ensure the signal is sufficiently large in amplitude so as to overcome interference from noise, and thus facilitate operation of the probe. Aside from serving as one half of the capacitor that induces the generation of the current signal from the KP vibration over the concrete surface, the disk also serves as a crude antenna which receives “noise” from the environment. Noise is undesired signals that come from a variety of sources that include ac emissions from electric lighting and power lines, spurious radio frequency signals, etc. that compete with the signal. The ratio of the amplitude of the desired signal to the noise is called the signal-to-noise ratio, and if the ratio is too small, it will cause the true current signal to become indiscernible. This situation can be addressed in a variety of ways; for the scaled-up KP it was done by the introduction of a Faraday Shield and filtration of the current signal. As mentioned in Section 2.4, the Faraday Shield effectively isolates the disk from the surrounding environment [15], and the filters (bandstop and bandpass) remove most spurious signals of frequencies away from that of the vibration frequency of the disk.

2.3 Probe Control System

In the small scale laboratory experiment (Section 3.1) signal processing was performed via an analog circuitry configuration used in the prior experimentation performed by [1] for the initial small-scale laboratory units they developed. The analog circuitry proved sufficient for the small scale laboratory testing, however when moving to the large probe, a digital processing system proves to be more advantageous. This is because more features and controls can be implemented with a digital processing system, along with the fact that the ease of commercial replication increases substantially.

To that end, a data processing unit (DPS) was developed that determines the nulling voltage to be applied (V_a), logs the data from the scans, and performs additional secondary functions (such as measuring the gap between the disk and the concrete). Data acquisition is performed by means of a Measurement Computing USB 1608 FS-Plus acquisition board. The data is imported and then processed by means of a LabVIEW™ code and the corresponding potential difference is applied via a Measurement Computing USB 3101 FS Analog Output Board. Figure 10 below illustrates the components of the DPS.

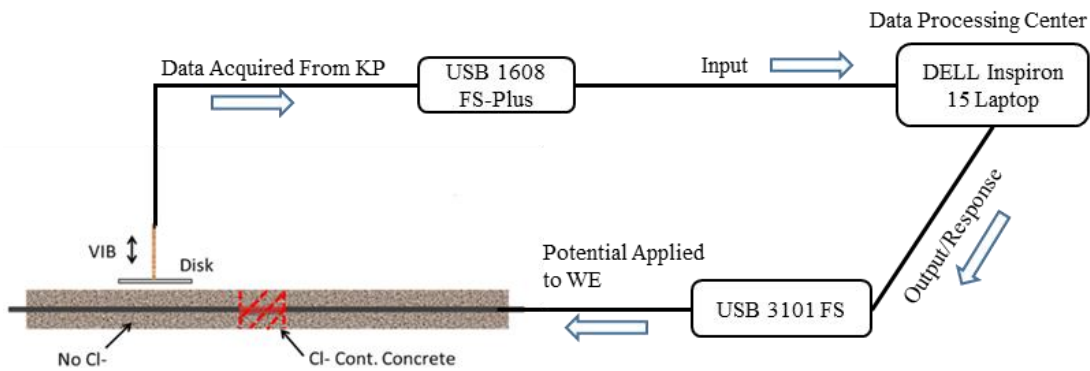


Figure 10-DPS schematic outlining the major components and their relation to each other.

LabVIEW code was written to perform the processing of the current signal acquired from the sensing disk and to generate the corresponding direct current potential required (V_a) for nulling. The block diagram of the code used in the data processing unit is shown in Figure 11 below. Figure 12 illustrates the condition that indicates a nulling potential has been applied. An explanation of the code main functions follows.

The front end acquires via the vibrating disk a current signal $I(t)$ per Eq.(10), applied by the front end circuit. A signal proportional to excitation vibration signal for the disk is also fed into the control system. The phase difference between both signals is measured and used to determine in which direction the DC nulling potential needs to be applied. The amount by which

the nulling potential is applied is increased proportional to the amplitude of $I(t)$, via a proportionality constant K . Further processing is described next.

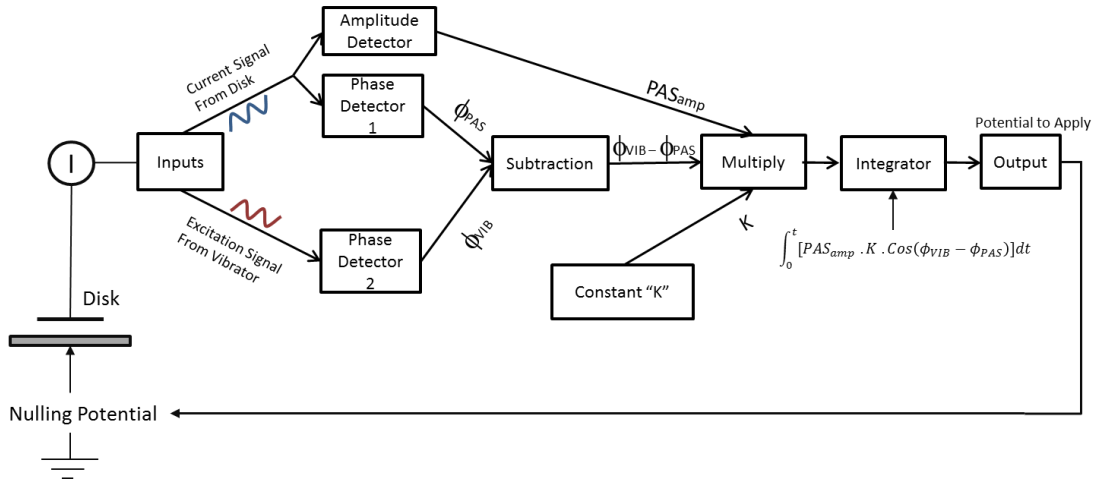


Figure 11-Block diagram of the LabVIEW™ code. The inputs to the system are the current signal from the disk and the excitation signal from the vibrator that is used as a reference for phase changes. The output is the potential needed to apply to the rebar in the case of a bridge deck scan.

As the KP control units applies potentials that transition around the null potential V_a , the nulling signal shifts from 0 degrees to plus 180 degrees (where the cosine of the difference of phase angles changes from 1 to -1). The changes tend to occur back and forth rapidly as each correction will shift polarity causing the applied potential to oscillate around V_a . This is shown graphically in Figure 12.

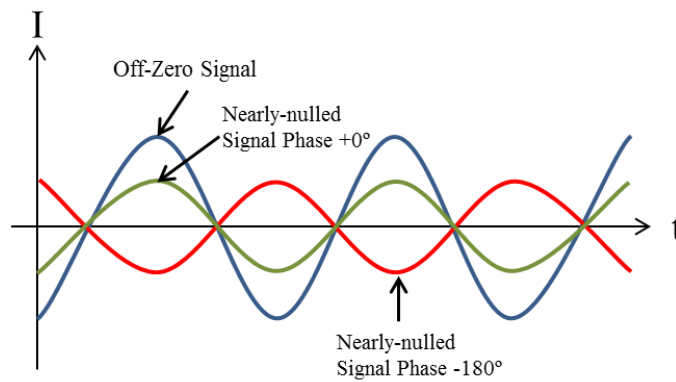


Figure 12-Nulling zero process. The KP initially is off-zero (blue signal) and the corrections fluctuate between the red and green curves representing the direction the signal is applied.

To dampen oscillations of the nulling signal around V_a , the code includes functions that average the effect of the phase changes, equivalent to Eq.(12).

$$V_a = \int_0^t [PAS_{amp} \cdot K \cdot \cos(\phi_{VIB} - \phi_{PAS})] dt \quad (12)$$

where PAS_{amp} is the amplitude of the current signal acquired at the preamplifier which will approach zero as the nulling potential V_a approaches the natural potential V_n in magnitude, the K term in the equation is a proportionality constant that controls the rise time of the DC response signal, and the last term performs the cosine of the difference in phase between the preamplifier signal and the excitation (vibrating) signal (giving the correction calculated per time interval a polarity when added to the previous sum). The above equation is calculated every 25 mS in the DPS and as such a new DC potential is applied at the same rate. To prevent sharp changes in the potential difference applied, the DC potentials calculated are integrated, wherein the current value is added to the cumulative sum of the prior values before being sent out.

2.4 Probe Design

Incorporating the elements from the previous sections, the scaled-up KP prototype was built to the following specifications. Figures 13 through 17 are a series of images of the prototype.

- 10 cm galvanized steel mesh sensing disk
- Vibration frequency: 160 Hz
- Vibration amplitude ~ 0.3 mm peak-to-peak
- Time constant $\tau \sim 0.3s$ (see Section 2.5)
- Operating gap 1 cm typical, to 2 cm max

- Traveling speed: 0.6 mph (walking speed)
- Wheel diameter/base : 10 cm/28 cm
- Electronic control: Integrated cordless operation with Windows laptop

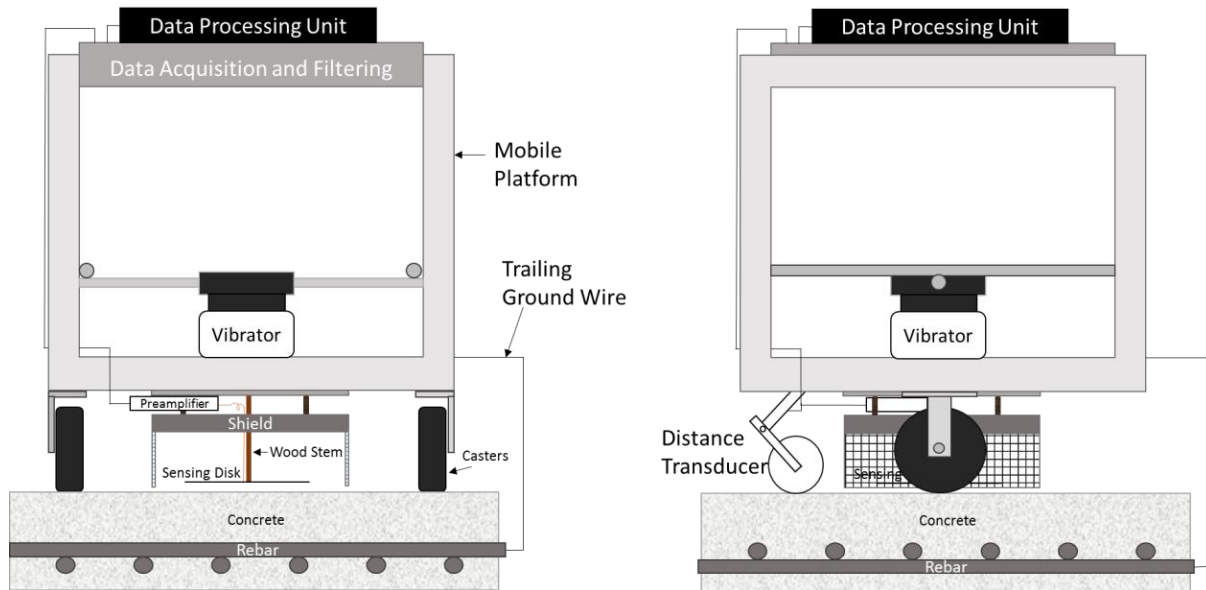


Figure 13-Schematic of the KP Prototype emphasizing major components. The left image is a front view and the right image is a side view. The shield has been partially cutout in the front view image to facilitate clarity in seeing the sensing disk and wood stem. The trailing ground wire is the sole connection between the KP and the rebar assembly.



Figure 14- KP on concrete slab with emphasis on Data Processing Unit. Note the following items in the picture, the data processing unit (laptop) and the trailing wire connecting to the rebar mat.

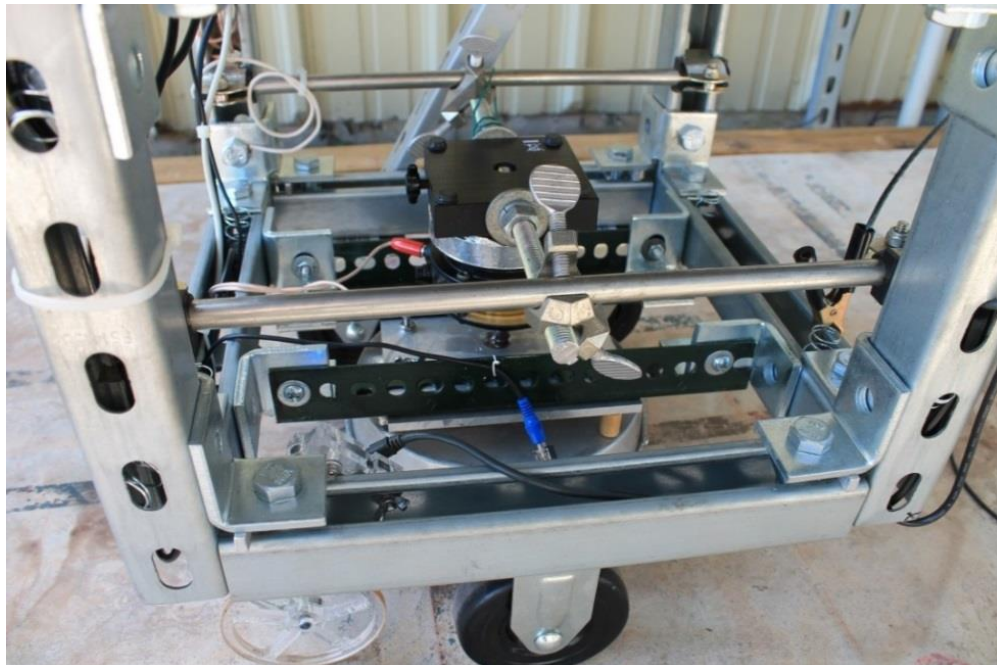


Figure 15-The vibrator and other key frame components.



Figure 16- Photo of the underside of the KP. Note the preamplifier (shown with three wires connected), along with the shield and the sensing disk over the concrete.

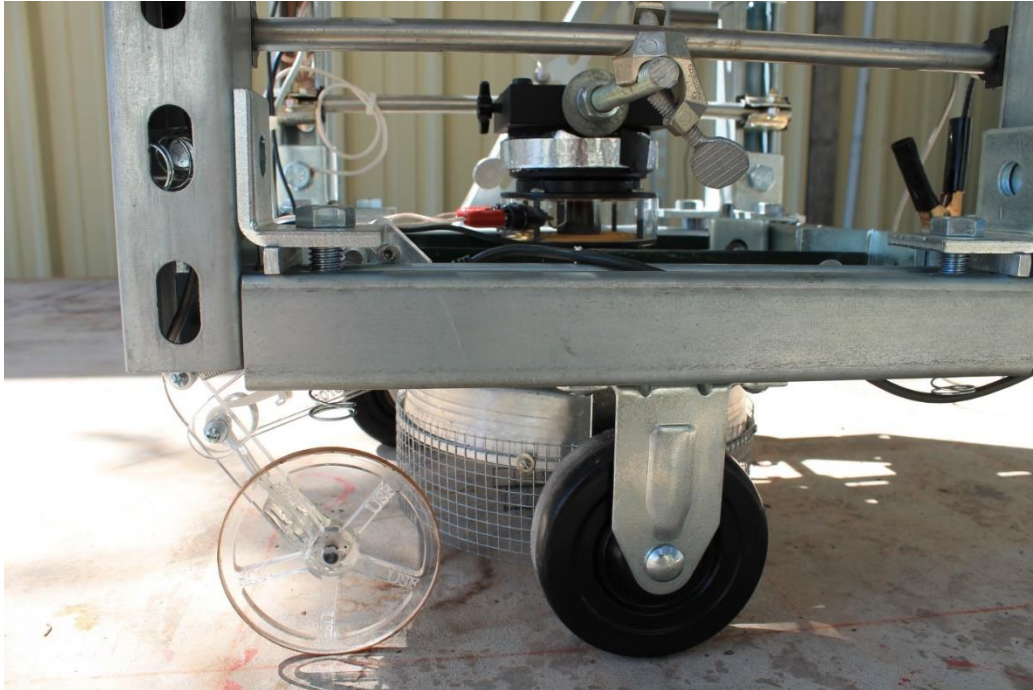


Figure 17-Distance transducer. The distance transducer was made by Dr. Celestin from the University of South Florida that determines the distance traveled.

2.5 Dynamic Probe Response and Proposed Method for Further Signal Processing

The KP that is being developed under the project of which this thesis is a part of, is intended for highway applications as part of a moving vehicle. Therefore the speed of probe response to changes in the potential of the surface beneath the moving disk is important as slow response would limit test speed accordingly. Consider for example the case of the probe travelling over a portion of a bridge deck where the potential changes abruptly from a given value on a part A of the bridge to another value in an immediately adjacent portion B. The effect is the same as a sudden change in the potential of the surface beneath the sensing disk. On first approximation the response of the probe to such a potential step function around a moment $t=0$ when the step takes place would be equivalent to a simple time constant function of the type adapted from [17]:

$$Em(t) = \alpha + (\beta - \alpha)(1 - e^{-\frac{t}{\tau}}) \quad (13)$$

where $Em(t)$ is the potential measured by the probe at any given time, α is the potential on part A just before the step, β is the potential on part B, and τ is the characteristic time of the system. Effectively, the system responds to a unit voltage step with a time dependent response function [17]:

$$A(t) = (1 - e^{-\frac{t}{\tau}}) \quad (14)$$

Given the properties of the exponential function, τ is the amount of time required for the measured potential to change by a fraction $1-e^{-1}$ (~63%) of the value of the step ($\beta-\alpha$).

The value of τ can be obtained experimentally by placing a metal plate beneath the disk, abruptly changing the plate potential, recording the KP output, and fitting it by means of Eq. (10). The process described was employed and the results are shown in Figure 18 below.

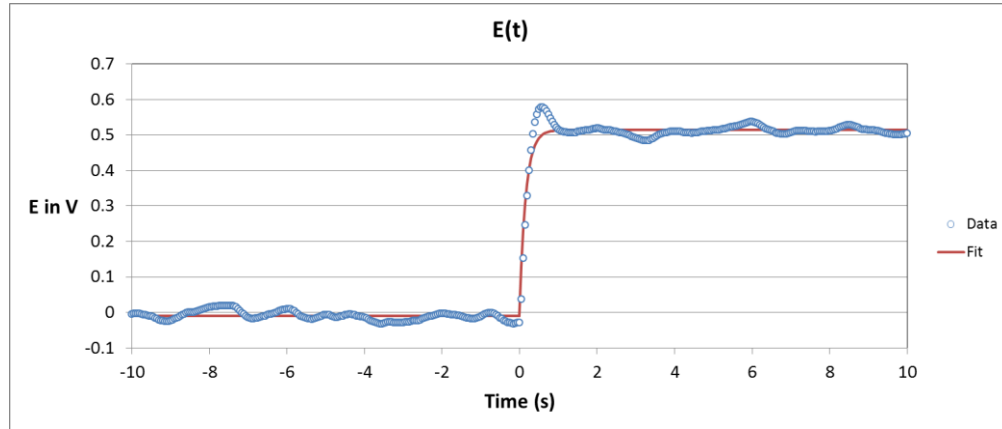


Figure 18- Probe-time response for a potential step. The measured data of the system along with a least squared error fitting of Eq. (13) to the observed results. In the case of the test run, A was about 0 V and B which represents the other portion of the bridge deck was simulated as being 0.5 V. The τ was 0.16 seconds, resulting in very little rounding of the step. The overshoot of the potential applied by the KP was neglected in the fitting at this time.

The response in Figure 18 is the convolution of the actual step surface potential profile with the dynamic probe response modeled by Eq. (13), and the addition of some random noise. A means of deconvolution of the actual potential profile from the KP output profile is proposed in the subsection below, however it was not implemented in actual testing but is reserved for future work.

2.5.1 Proposed Method for Improved Signal Processing

Suppose for the conditions above (two portions of a bridge deck with different potentials) that the potential profile along the bridge as the probe moves (assuming for simplicity at a constant speed) is found to be $E_m(t)$ and the actual potential profile as an equivalent function of time is $E'(t)$ in Figure 19 below.

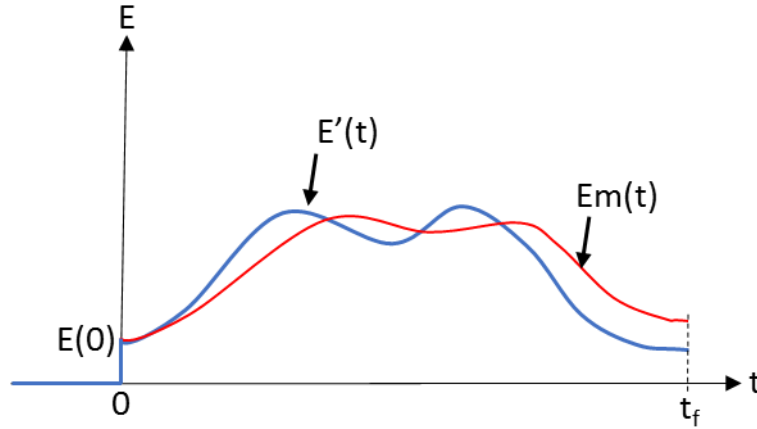


Figure 19- Measured potential profile versus actual potential profile. $E_m(t)$ is the potential profile measured by the KP whereas $E'(t)$ is the actual (time equivalent) potential profile.

The next step in the deconvolution process is to propose a function that represents the time dependent response of the KP, which convoluted the $E'(t)$ profile. Figure 20 below will be used as the time dependent response of the signal; it is modeled off of Figure 18 and Eq. (13).

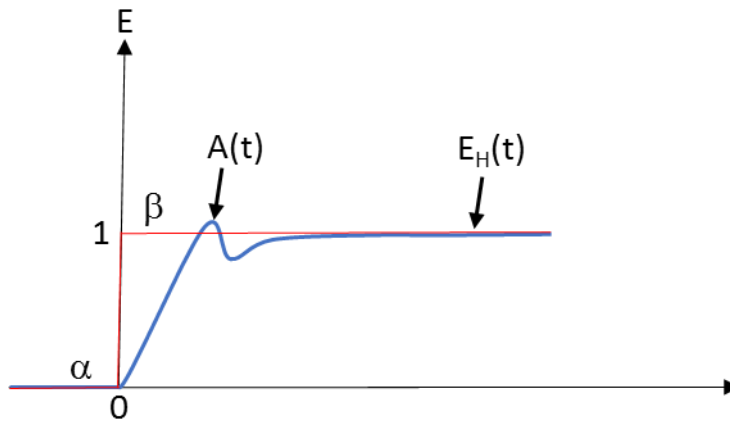


Figure 20- Probe-time response schematic. Note that the step $(\beta - \alpha)$ described in the preceding section is represented as having a magnitude of 1 and is given the designation $E_H(t)$, $A(t)$ describes the probe's signal as a function of time.

An expression can be written that describes the potential as a function of time for both the actual potential profile and the measured potential profile, which are presented as Eq.'s (15) and (16) respectively.

$$E'(t_f) = E(0) + \sum_{i=1}^f \Delta E'(t_i) \quad (15)$$

$$E_m(t) = E(0)A(t - t_0) + \sum_{i=1}^f \Delta E'(t_i)A(t - t_i) \quad (16)$$

There the measured potential profile is represented by a sum of small step functions starting at progressively increasing moments t_i , each step of amplitude $A(t-t_i)$ which follows the system response function described in Section 2.5. The summation operator as presented can be translated directly into integral notation as shown in Eq. (17), the resulting equation is presented in [18].

$$E_m(t) = E(0)A(t - t_0) + \int_0^t \frac{dE'(m)}{dm} A(t - m) dm \quad (17)$$

Eq. (17) can be shown to be equivalent to the following form as demonstrated by [18].

$$E_m(t) = E(0)A(t - t_0) + \int_0^t E'(m) \left\{ \frac{d}{dt} A(t - m) \right\} dm \quad (18)$$

Evaluating the integrand in Eq.(18) will yield an expression that represents the convolution of $E(t)$ and $dA(t)/dt$ [19]:

$$E_m(t) = E(0)A(t - t_0) + (E'(t)) \left(\frac{dA(t)}{dt} \right) \quad (19)$$

When convolution occurs in the context of this problem, it can be treated in simplified terms via Fourier transformations. Specifically, the Fourier Transform of the convoluted signal is equivalent to the multiplication of the Fourier Transforms of the un-convoluted signal and the convoluting, a result commonly described as the Convolution Property [19]:

$$F(P * Q) = F(P) F(Q) \quad (20)$$

where F represents the Fourier transform of the term in parenthesis.

The Fourier Transform as described by Feynman [20], divides a continuous waveform with a given period into a frequency-amplitude spectrum comprised of the frequencies of cosine waves with corresponding amplitudes (representing the power of the waveform) that when added together form the continuous waveform [20]. To ensure the potential profile measured by the KP is considered a continuous waveform, a finite number of zeroes will be added before and after, thereby “windowing” [19] the section and causing the first term of Eq. (19) to become nulled. Eq. (21) shows how the application of the Convolution Property of Fourier Transforms to Eq. (19).

$$F(E_m(t)) = F(E'(t))F\left(\frac{d}{dt}A(t)\right) \quad (21)$$

Performing algebraic manipulation of Eq. (22) yields the final equation of interest that is proposed for the deconvolution process [18].

$$E'(t) = F^{-1}\left(\frac{F(E_m(t))}{F\left(\frac{d}{dt}A(t)\right)}\right) \quad (22)$$

where F^{-1} represents the inverse Fourier transform operation [19].

Eq.(22) would be applied to a windowed potential profile measured by the KP over the bridge deck or similar surface to be assessed. Doing so would allow for faster travel speed for the Kelvin Probe assembly, effectively sharpening the measured potential profile that had been “blunted” by the finite probe response speed, thus allowing for better identification of the corroding spots on the bridge deck. This process has not been applied to the potential profiles

presented in this thesis, but it is an important component of further probe development now in progress, so a description has been included here as an initial step in that development.

CHAPTER 3: LABORATORY SCALE INDOOR TESTING

3.1 Laboratory Testing on Concrete Slabs

For initial testing the scaled-up sensing arrangement was mounted in a stationary manner with a movable specimen underneath (Figures 21 and 22). These tests were made with a preexisting analog control unit, but are nevertheless relevant to the overall probe operation and functionality. Two available concrete slabs (Figure 21) 70 cm long, 15 cm wide and 5 cm thick, each with one #3 (0.95 cm diameter) steel rebar placed longitudinally on center, with the concrete in the central ~5cm of the slab contaminated with Cl⁻ ions to induce active corrosion of the rebar there, while the rest of the rebar surface remained in the passive condition. Detailed description of the slabs is given in [1].

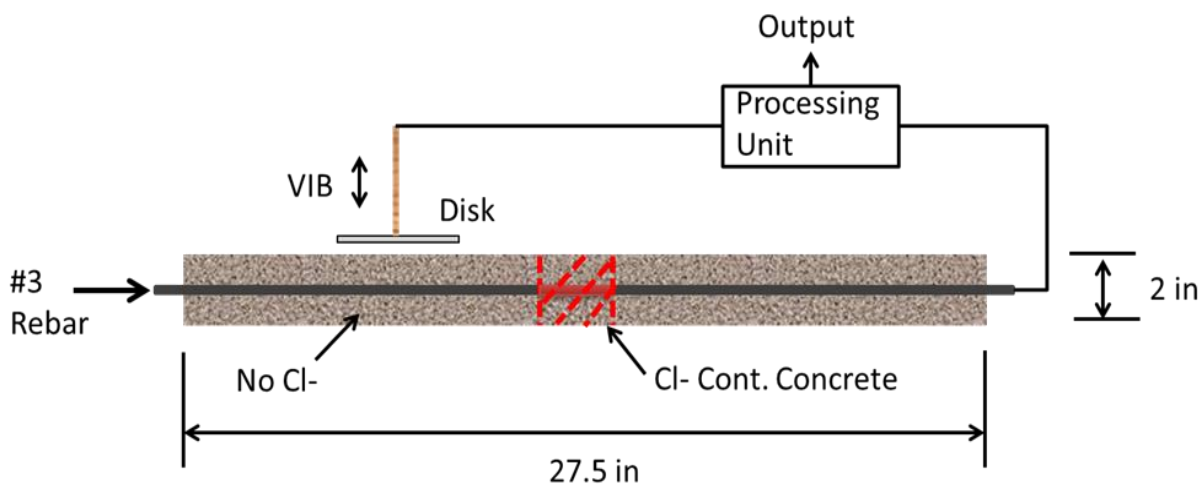


Figure 21-Schematic of the laboratory experimental setup.

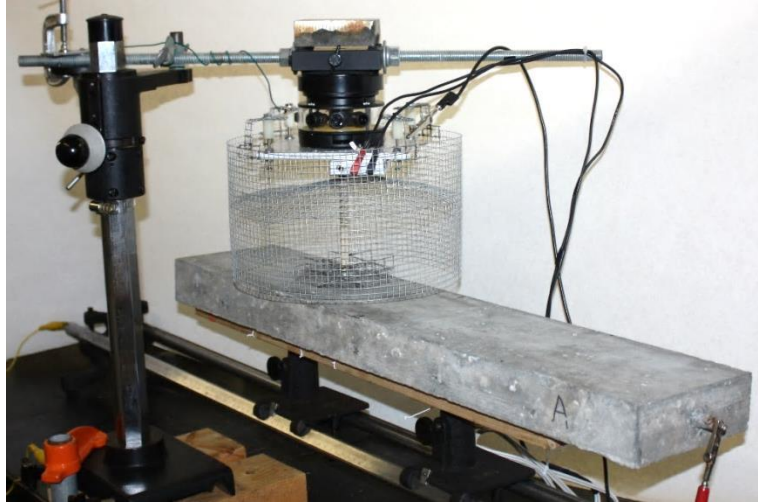


Figure 22-Laboratory concrete beam test setup. The rebar and its connecting point is seen emerging at right end of slab. Disk assembly is stationary while longitudinal position is changed by sliding slab over the graduated rail. The sensing disk is surrounded by a grounded wire mesh electric shield ~25 cm in diameter. Vibrating assembly is located at the top; wires connect system to electronic driving and signal processing unit.

3.1.1 Laboratory Testing Experimental Objective and Methodology

The disk was positioned over the longitudinal centerline of the surface of the slab as shown in Figure 21. Vibration frequency was 80 Hz and vibration amplitude ~ 1mm. The disk-to-concrete surface distance was 1 cm and 2 cm at different test series. Potential readings were taken at 13 longitudinal positions at 5 cm intervals, starting with the left disk edge directly above the left end of the slab. Disk position was recorded as the distance of the disk axis from the left end of the slab; slab center (corroding region) was thus at disk position= 35 cm.

The tests were performed on the two replicate slabs and on both the top and bottom sides of each slab. After the tests were finished on each side of a slab, an additional set of traditional-method potential readings was taken at each position using a Saturated Calomel Electrode (SCE) fitted with a moist sponge at the tip. KP readings were taken within ~ 5 seconds of placement at each new position. SCE readings were taken after waiting ~15 seconds after sponge contact with

the concrete to allow for a uniform degree of approach to stabilization of the potential, which for the traditional method is subject to drift as noted in [1].

3.1.2 Laboratory Testing Experimental Results

Results for tests conducted ~ 1 day after removal of both slabs from their 100% R.H. storage container are exemplified in Figure 23 for the top-side potential measurements of each slab. Bottom-side results were comparable to those shown here. The results demonstrate that the scaled up KP sensing system was functional over concrete surfaces, and able to identify for both slabs the central corrosion location via the lowest point of the potential profile. The identification was consistent with that of the traditional method using the wet-tip SCE. The offset between the KP and wet-tip electrode potential readings was generally consistently uniform and suitable for calibration of the KP if absolute potential measurements were desired. These findings are in agreement with those obtained for the miniature KP system used while initially developing the concept [1].

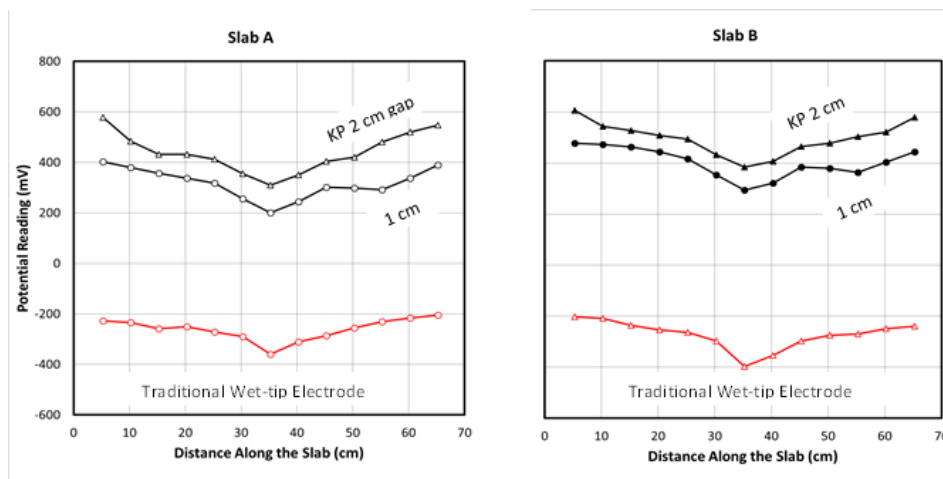


Figure 23-Potential profiling. Potential scans of replicate slabs obtained with the KP operating at two disk-to-concrete surface gaps (1 cm and 2 cm (~3/8 in and 3/4 in)), and with the traditional SCE wet-tip electrode method. The corroding region was located at the center of each slab (35 cm position).

The results also demonstrate that the KP was able to operate successfully at an appreciably large, 2 cm (~ 3/4 in) gap (20 times greater than that used in the initial miniature unit) between disk and concrete surface. This finding is important as the ability to operate with a gap of such size, which is significantly greater than the typical short term deck surface roughness amplitude, was a necessary requirement for practical use of the product of this project. It is also noted that the KP was able to show good spatial resolution with a sharp minimum potential location even though the disk diameter was equal to two sampling spaces, and even when operating at the 2 cm (~3/4 in) gap. This observation indicates that the sampled footprint is reasonably confined under the conditions evaluated so far.

The results in Figure 23 also show that the potential profiles for 1 cm and 2 cm (~3/8 in to 3/4 in) gap sizes were offset from each other by a nearly fixed value of ~100 mV while retaining similar shapes, suggesting that a potential-to-gap functional dependence of ~ 0.1 V / cm exists at least for the potential and distance ranges examined. An important outcome of that observation is that, in the regular operation mode anticipated for the probe, it does not appear to be necessary to perform fine physical real time control of gap distance when a vehicle mounted probe is moved over the deck surface. Rather, an auxiliary ultrasonic, electronic or optical disk to-concrete distance sensor could be used to provide real time topography information as the concrete surface is scanned. That information could then be applied to numerically correct the probe potential readings to compensate for gap variations once a preliminary functional dependence is established beforehand. Short-term reproducibility tests were conducted by performing multiple consecutive profile measurements on one of the slabs, with results shown in Figure 24.

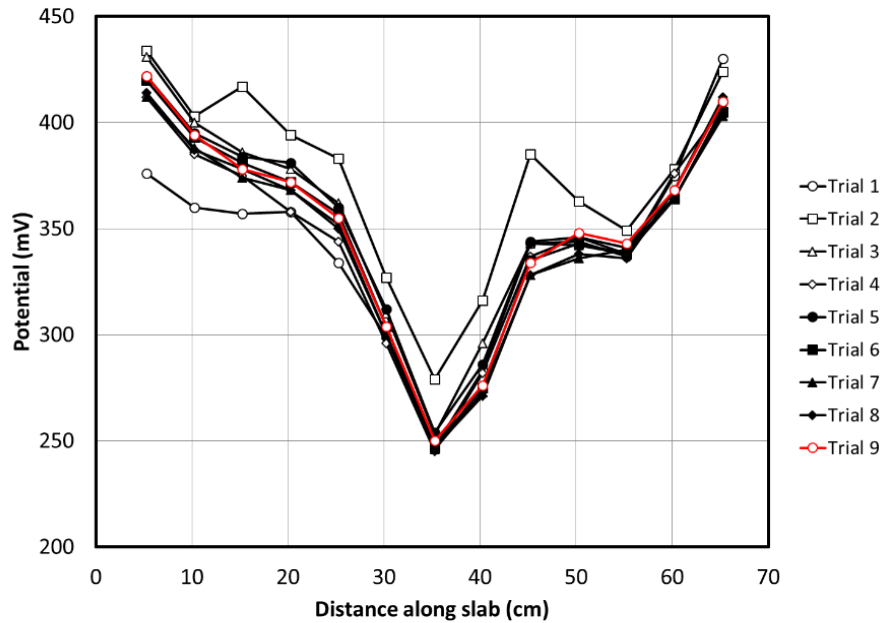


Figure 24-Short term reproducibility tests. Vertical scale expanded to emphasize test-to-test deviations.

The tests revealed that under the present implementation there was a good degree of reproducibility of potential scans, providing identification of the corroding spot in all trials. The average standard deviation around the average of the entire set of 9 potential readings obtained at each position was only ~12 mV. However, the tests also revealed some instances (trials 1 and 2) where some temporary and nearly systematic potential reading offsets occurred over some of the slab positions tested. The average standard deviation for the rest of the trials was only ~5.3 mV.

CHAPTER 4: OUTDOOR LARGE SCALE TESTING

4.1 Potential Map Generation

An approximately 8ft by 8ft instrumented reinforced concrete test slab apparatus at the University of South Florida was used for the initial test of the mobile KP prototype (MKPP). The slab has 15 # 4 rebars equispaced at 6 inches on center that can be electrically interconnected with one another. Some of the bars are further split into segments interconnectable as well. The test configuration used is shown in Figure 25 and described in detail later.

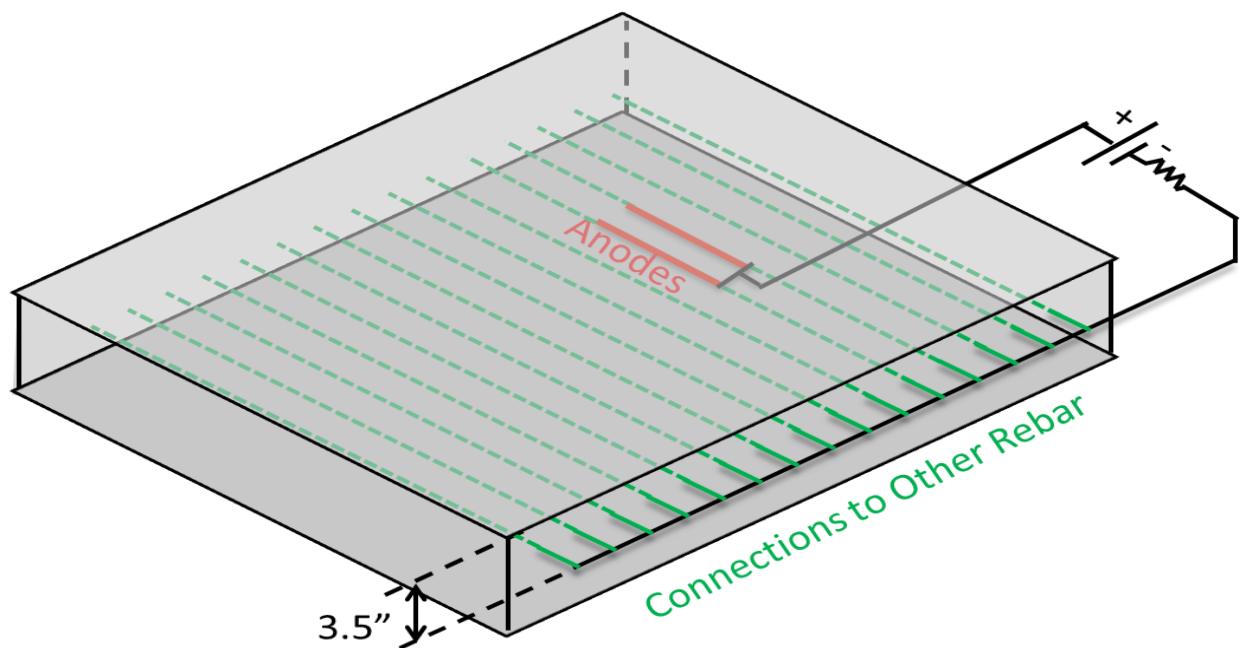


Figure 25-Instrumented test slab schematic. The areas denoted as anodes were the simulated corroding spots and will be described further below.

Figure 26 shows the slab in situ along with the MKPP placed as would be during potential mapping.



Figure 26-Photo of the testing apparatus with the MKPP.

The arrangement allows, via an external current source, to temporarily convert different parts of the system into anodic or cathodic regions, thus simulating a wide variety of equivalent corrosion location scenarios with corresponding actual potential distributions on the top surface. Those potential distributions can then be sampled with the MKPP or with conventional electrodes, creating a variety of data sets to evaluate and demonstrate probe functionality.

The MKPP scanning was performed by a single operator that pulled the probe along one of the 9 main row gridlines while another person tensioned the trailing wire that provides the ground connection between the rebar mat and the MKPP, as the probe moved along at ~ 0.6 mph. Figure 27 below shows the scenario described above.



Figure 27-Setup employed when scanning the reinforced concrete slab. The probe operator is seen to the left, and the person holding the trailing wire (right) will eventually be replaced by an automatically spooling wire. At the end of each row the probe was picked up and shifted to the next row and the next scan was initiated.

4.1.1 Potential Map Generation Results

A 10.25" square grid was placed on the instrumented test slab starting 4" from the edge of the slab in all directions. The 4" offset was used to ensure that the MKPP sensing disk would be completely over the concrete slab (instead of part being over the wood skirt) for the entirety of the potential mapping. The grid was calibrated so as to have an integer number of points on the remainder of the slab scanning area, which corresponded to a grid with 81 vertices (9 by 9). The intersections of gridlines were the sites where the traditional wet-tip electrode potential measurements were taken, whereas entire rows were scanned continuously (at an average speed of 0.6 mph) with the MKPP prototype. The continuous MKPP scan data was then discretized to the same 81 points as the CSE map to allow for comparison with the results from the traditional method.

The first maps generated were baselines wherein the entire rebar mat was interconnected (including the sites that would become anodes later on in the testing see in Figure 25). It was

expected that the potential map would have few points of markedly different surface potential than the surrounding areas. The slab was scanned a total of four times (twice in each direction in each of the nine lines sampled) in the case of the MKPP, and mapped twice using the traditional method as well. After performing the baseline scans, two 3 foot long rebars were artificially made anodes by means of galvanostatic polarization (about 4 mA, corresponding to a current density of about $5.5 \mu\text{A}/\text{cm}^2$) as shown by the red lines in Figure 25. It was expected that the polarized rebar would simulate a corroding spot, whereas the rest of the rebar mat would appear to be passive. The slab was scanned in this polarized condition four times by the MKPP and mapped twice by the traditional method.

The four scans per row for each slab configuration (baseline, polarized) recorder by the MKPP was then averaged and the one single map was generated by compiling the potential profiles. Figure 28 shows a sample averaged potential profile.

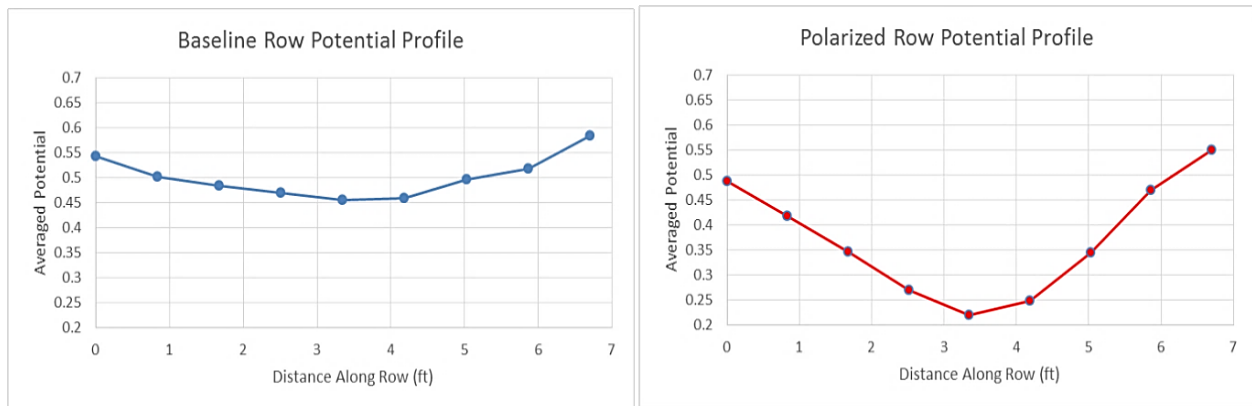


Figure 28- For a given row of the slab the above potential profiles were measured using the MKPP. The baseline profile (left) represents the rebar mat without corrosion. The polarized profile (right) represents the same row's surface potentials when the rebars simulating a corroding spot were polarized. Within the potential profiles, the marker points are those used to generate the potential maps. The marker points also represent spatially where the traditional method mapping measurements were taken as well. Note the substantially more negative potential observed in the middle of the polarized profile, indicative of the location of the corroding spot.

Compiling the potential profiles in potential maps yields the following results.

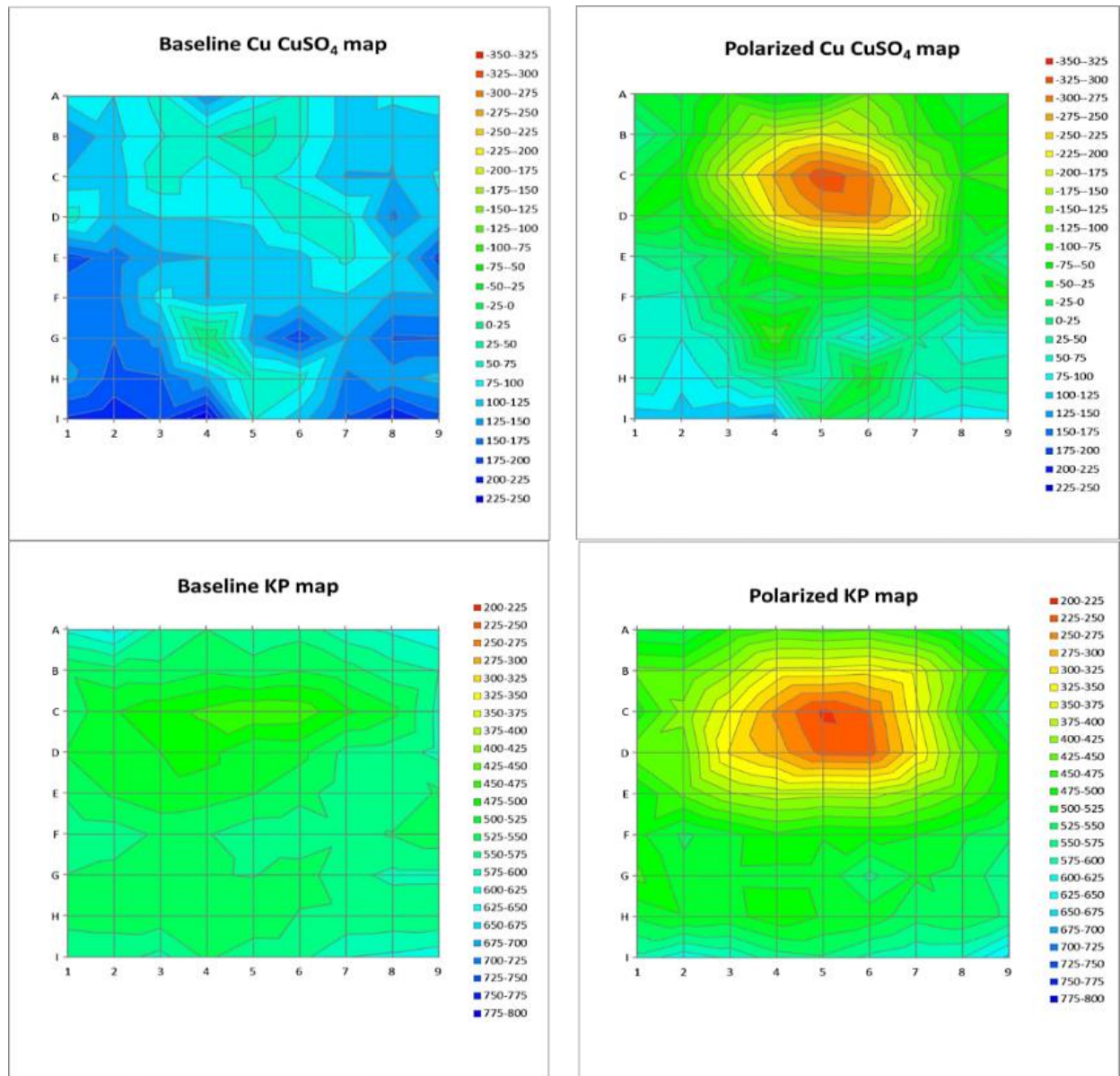


Figure 29-Potential maps generated using the MKPP and traditional method. Each row and column indicator corresponded to the intersection of the 10.25” square grid. The corroding spot (red) is approximately at grid intersection C5 for both polarized maps.

The results in Figure 29 are highly encouraging. In the absence of rebar polarization the KP showed as expected a flat potential profile, in agreement with that obtained with the CSE

electrode in the same condition. On the polarized system the contactless MKPP measurements showed a distinct differential potential profile identifying the position of the temporarily anodic segments, and in excellent agreement in both locations and high-to-low potential difference in the comparable profile obtained with the traditional CSE method.

Additionally, Figure 29 supports the conclusion that the Kelvin Probe can successfully identify a corroding spot even when moving at 0.6 mph (~1 ft/s). The Kelvin Probe was able to scan the area of the concrete slab in about ~3 minutes, whereas the same area was scanned with the traditional method in ~30 minutes, even after permitting only 10 seconds of CSE stabilization time. Therefore, the MKPP was able to scan the surface continuously at a rate 10 times faster than the traditional method while still successfully identifying the corroding spot.

The MKPP was not subject to junction potentials and the results from the multiple scans showed the potential measurements are highly reproducible. If the improved deconvolution signal processing proposed in Section 2.5.1 was implemented, reproducibility may be even further improved.

Also, in prior work [21], the MKPP was used to perform scans identical to those described in this chapter except at a different polarization level ($2 \mu\text{A}/\text{cm}^2$) and instead of scanning in a continuous movement from one side of the slab to the other, the probe measured the potential of the concrete surface only on the same grid points as the CSE mapping. Figure 30 is a graphical representation of that comparison, showing that for the reference disk material used (galvanized steel) a nominal calibration offset of 715 mV could be used to translate the MKPP readings to comparable CSE measurements.

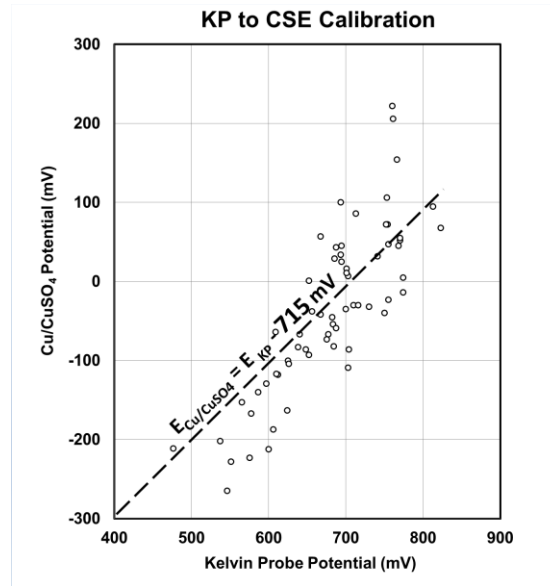


Figure 30-Sample calibration from previous scanning of the concrete slab under similar conditions.

It is emphasized that the offset value is for the specific condition examined and not a universal translation parameter, however the same approach could be implemented on the scans presented in this thesis and an absolute calibration of the KP disk to the CSE could be made. It is also noted that for both the MKPP and the CSE data a certain amount of experimental scatter exists, as it is well known that interpretation of potential maps requires consideration of the entire map and not on single individual values.

Additionally, if the concept of an assembly of multiple probes presented at the end of the Introduction was implemented, this could appreciably impact and improve current bridge deck scanning practice by allowing bridge decks to be scanned without closing lanes, by one operator, and in a time inconceivable when using the traditional method.

Also, future work will focus in increasing the rate of travel of the MKPP over the concrete surface that still provides useful corroding spot identification, to potentially allow for scanning at highway speeds.

CHAPTER 5: SUMMARY OF FINDINGS

- A scaled-up Kelvin Probe was constructed that achieved the target goals such as enlarging the sensing disk to 10 cm, increasing the disk-to-concrete surface gap to 1 cm for outdoors testing and as much as ~2 cm for indoor laboratory experiments. Additionally, other aspects such as the electromagnetic driving unit were scaled (to a commercially available vibrator operation) [22] and a suitable mobile frame was constructed to allow for a rugged KP configuration suitable for an actual road surface.
- Laboratory tests with the probe showed that corrections for operating gap changes may be conducted by appropriate calibration.
- Laboratory tests demonstrated the new KP prototype was capable of generating potential profiles in a fast and highly reproducible manner. The profiles were consistent with those made using the traditional method
- The probe was mounted in a rugged rolling platform, and was configured such that all necessary components for operation (with exception of the trailing wire) were self-contained.
- Successful test runs were conducted with the mobile KP prototype (MKPP) on a large instrumented concrete test slab simulating a bridge deck. The MKPP's potential maps on the outdoor slab successfully identified the anodic spot in the slab and provided information in excellent graphic agreement with maps obtained by conventional CSE electrode surveys.

- A method for calibrating potential maps generated by the MKPP to the results from the traditional method was presented.
- A deconvolution signal processing method was proposed that may enable the probe to be run at faster speeds while still getting useable data.
- The MKPP was able to scan each row of the concrete slab continuously at an average speed of 0.6 mph. Scanning the entire slab using the MKPP took ~3 min as opposed to the ~30 minutes it took to map the slab using the traditional method. Therefore, the KP mobile prototype was able to scan the slab in 1/10 the time required by the traditional method.
- Future work concepts such as constructing an array of probes capable of scanning an entire lane at once was presented.

REFERENCES

- [1] Sagiúés, A. A., and M. T. Walsh. 2012. 'Kelvin Probe Electrode for Contactless Potential Measurement On Concrete-Properties And Corrosion Profiling Application'. *Corrosion Science* 56: 26-35.
- [2] ACI Committee 224, 1997. 'Cracking Of Concrete Members In Direct Tension'. ACI 224.2R-92. Detroit, MI 48219: American Concrete Institute.
- [3] Tinnea, J. 2012. 'Corrosion Control Plan For Bridges'. A NACE International White Paper. Houston, TX: NACE International.
- [4] Kumar, M., A.M. ASCE, Z. Ma, and M. Matovu. 2014. 'Mechanical Properties of High-Strength Concrete'. Buffalo, NY: University at Buffalo.
- [5] Lee, S. K. 2012. 'Current State of Bridge Deterioration in the U.S. Parts 1 &2'. Materials Performance. NACE International, Vol. 51, No.1.
- [6] Koch, G. H., M. P.H. Brongers, N. G. Thompson, Y. P. Virmani, and J.H. Payer. 2002. 'Corrosion Costs and Preventive Strategies in the United States'. NACE International. Washington, DC: FHWA and NACE International. FHWA-RD-01-156
- [7] Federal Highway Administration,. 2006. 'Status of The Nation's Highways, Bridges, and Transit: 2006 Conditions And Performance'. Report to Congress, Washington, DC: FHWA.
- [8] ASTM C876-09. 2009. 'Standard Test Method for Half-Cell Potential of Uncoated Reinforcing Steel in Concrete'. West Conshohocken, PA: ASTM.
- [9] Fontana, M. 1987. 'Corrosion Engineering'. 3rd ed. New York, NY: McGraw-Hill
- [10] Gellings, P. 2005. 'Introduction to Corrosion Prevention and Control'. Enschede, Netherlands: University of Twente
- [11] Thomas, J G N. 2014. 'The Electrochemistry Of Corrosion'. Corrosion Guides. Teddington, UK: National Physics Laboratory.
- [12] Klein, U., W. Vollmann, and P.J. Abatti. 2003. 'Contact Potential Differences Measurement: Short History And Experimental Setup For Classroom Demonstration'. *IEEE Transactions On Education* 46: 338-344.

- [13] Senway, R. A., and J. W. Jewett. 2010. *Physics For Scientists And Engineers With Modern Physics*. 5th ed. Belmont, CA: Brooks/Cole Cengage Learning.
- [14] Provisional patent applications to the U.S. Patent and Trademark Office filed by USF on May 30, 2012 (with A. Sagüés and M. Walsh, Inventors) and March 4, 2013 (A. Sagüés). Also USF research proposal to the National Cooperative Highway Research Program on February 25, 2013 (A.Sagüés, P.I.)
- [15] Faraday, M.1836. ‘Experimental Researches in Electricity’. Vol 1. Reprinted from the *Philosophical Transactions* of 1831-1838. London: Richard and John Edward Taylor, Printers and Publishers to the University of London
- [16] Lamalle, P. U. 1997. ‘Capacitance Of An Array Of Thick Rods Parallel To The Ground-Application To The JET ICRF Antenna’. *Journal Of Physics D: Applied Physics* 30 (1).
- [17] Jones, R. V. 2002. ClassNotes. ‘Electronic Devices and Circuits’. Harvard University Course ES154, Fall Term 2001
- [18] Goldman, S. 1949. ‘Transformation Calculus and Electrical Transients’. Englewood Cliffs, NJ: PRENTICE-HALL, INC: 113-115.
- [19] Oppenheim, A. V. 2011. Class Notes. ‘Signals and Systems’. MIT OpenCourseWare, Spring Term 2011
- [20] Feynman, R., R. B.Leighton, and M. Sands.1963. ‘The Feynman Lectures on Physics, Vol. 1’. Reading, MA: Addison-Wesley Publishing Company
- [21] Sagüés, A. A, L. P. Emmenegger. 2015. ‘Stage 1 Report NCHRP-176 042615’. For project ‘Contactless Electrode for Fast Survey of Concrete Reinforcement Corrosion’ Idea Program Project 176. Presented to the National Cooperative Highway Research Program.
- [22] Emmenegger, L.P. 2014. ‘Kelvin Probe Electrode for Field Detection of Corrosion of Steel in Concrete’. Honors Thesis, University of South Florida: Tampa, FL